

Contents lists available at ScienceDirect

Computers and Mathematics with Applications

journal homepage: www.elsevier.com/locate/camwa





The time dimensional reduction method to determine the initial conditions without the knowledge of damping coefficients

Thuy T. Le a, Linh V. Nguyen b,*, Loc H. Nguyen c, Hyunha Park d

- ^a Department of Mathematics, NC State University, Raleigh, NC 27695, USA
- b Department of Mathematics, University of Idaho, 875 Perimeter Drive, Moscow, ID, 83844, USA
- c Department of Mathematics and Statistics, University of North Carolina at Charlotte, Charlotte, NC, 28223, USA
- ^d Department of Mathematics, George Washington University, 801 22nd St. NW, Washington, DC 20052, USA

ARTICLE INFO

ABSTRACT

Keywords:
Time reduction
Carleman contraction mapping
Initial condition
Damping coefficient

This paper aims to reconstruct the initial condition of a hyperbolic equation with an unknown damping coefficient. Our approach involves approximating the hyperbolic equation's solution by its truncated Fourier expansion in the time domain and using the recently developed polynomial-exponential basis. This truncation process facilitates the elimination of the time variable, consequently, yielding a system of quasi-linear elliptic equations. To globally solve the system without needing an accurate initial guess, we employ the Carleman contraction principle. We provide several numerical examples to illustrate the efficacy of our method. The method not only delivers precise solutions but also showcases remarkable computational efficiency.

1. Introduction

Let *T* be a positive number that represents the final time and let $d \ge 1$ be the spatial dimension. Let $u : \mathbb{R}^d \times [0, T] \to \mathbb{R}$ be the solution of

$$\begin{cases} u_{tt}(\mathbf{x},t) + a(\mathbf{x})u_{t}(\mathbf{x},t) = \Delta u(\mathbf{x},t) & (\mathbf{x},t) \in \mathbb{R}^{d} \times (0,T] \\ u(\mathbf{x},0) = f(\mathbf{x}) & \mathbf{x} \in \mathbb{R}^{d}, \\ u_{t}(\mathbf{x},0) = -a(\mathbf{x})f(\mathbf{x}) & \mathbf{x} \in \mathbb{R}^{d}. \end{cases}$$

$$(1.1)$$

We are interested in the following inverse problem.

Problem 1.1. Let Ω be a bounded domain of \mathbb{R}^d with a smooth boundary. Assume that $|f(\mathbf{x})| > 0$ for all $\mathbf{x} \in \Omega$. Given the measurement of lateral data

$$p(\mathbf{x},t) = u(\mathbf{x},t)$$
 and $q(\mathbf{x},t) = \partial_{\nu}u(\mathbf{x},t)$ (1.2)

for all $(\mathbf{x}, t) \in \partial \Omega \times [0, T]$, determine the function $f(\mathbf{x})$ for $\mathbf{x} \in \Omega$.

Problem 1.1 is an important problem arising from bio-medical imaging, called thermo/photo-acoustics tomography (see, e.g., [44,45,69,79,25,24]). One sends non-ionizing laser pulses or microwave to a biological tissue under inspection (for instance, woman's breast in mamography). A part of the energy will be absorbed and converted into heat, causing a thermal expansion and a subsequence ultrasonic wave propagating in space. The ultrasonic pressures u on a surface around the tissue are measured. Although the Neumann data $\partial_v u$ are not directly measured in the experiment, one can find it by solving the external hyperbolic equation [11]. Finding the initial pressure f from these measurements yields helpful structural information of the tissue. Most of the current publications focus on standard models with non-damping and isotropic media. The methods include explicit reconstruction formulas in [10-12,26,13,57,66], the time reversal method [20,21,23,75,76], the quasi-reversibility method [9,52] and

E-mail addresses: tle9@ncsu.edu (T.T. Le), lnguyen@uidaho.edu (L.V. Nguyen), loc.nguyen@charlotte.edu (L.H. Nguyen), hpark0@gwu.edu (H. Park).

^{*} Corresponding author.

the iterative methods [73,22,72,6,14]. The reader can find publications about thermo/photo-acoustics tomography for more sophisticated model involving a damping term or attenuation term [1–3,8,15,16,19,42,43,56,63].

The model under investigation (1.1) and Problem 1.1 were studied in [19,70,15,71]. However, in those works, the absorption coefficient $a(\mathbf{x})$ was known for every point $\mathbf{x} \in \Omega$. In this paper, in contrast, we assume that $a(\mathbf{x})$ is unknown. Since our focus is the inverse problem, we assume that (1.2) has a unique solution $u(\mathbf{x}, t)$. Assume further that this solution is bounded; i.e. there is an M > 0 such that

$$|u(\mathbf{x},t)| < M \quad \text{for all } (\mathbf{x},t) \in \mathbb{R}^d \times [0,T]. \tag{1.3}$$

Solving Problem 1.1 when a is known is possible, see [19,70,15,71]. However, the problem becomes challenging and interesting when a is not known.

- 1. Regarding "challenging", the challenge at hand stems from the necessity of computing two unknown functions, a and u while there is only one single governing equation, the hyperbolic equation in (1.1). Additionally, the product $a(\mathbf{x})u_t(\mathbf{x},t)$ in (1.1) adds nonlinearity to Problem 1.1. Solving nonlinear problems without providing a good initial guess poses an intriguing and scientifically significant challenge for the community. We propose to use a recently developed method, the Carleman contraction mapping method, that quickly delivers reliable solutions without requesting such a good initial guess, see [48,50,62]. This new method is designed based on the fixed-point iteration, the contraction principle, and a suitable Carleman estimate.
- 2. Regarding "interesting", in real-world applications, the function $a(\mathbf{x})$ is typically unknown as it represents the value of the damping coefficient at an internal point \mathbf{x} in Ω where one has no access. Therefore, being able to solve Problem 1.1 without requesting the knowledge of this internal data is a substantial contribution to the field. To the best of our knowledge, this is the first work that tackles this problem. A similar problem, which is to reconstruct the initial pressure with unknown sound speed has been studied theoretically (see [21,77,78,54]) and numerically (e.g., [80,55]). However, theoretically sound numerical approach for this problem is still out-of-reach.

Due to the lack of knowledge of the coefficient a, Problem 1.1 becomes nonlinear. Conventional approaches to computing solutions to nonlinear inverse problems typically rely on optimization techniques. However, these methods are local in nature, meaning they yield solutions only if good initial approximations of the true solutions are provided. Even in this case, local convergence is not guaranteed unless certain additional conditions are met. For a condition ensuring the local convergence of the optimization method employing Landweber iteration, we direct the reader to [17]. There is a general framework to globally solve nonlinear inverse problems, called convexification. The main idea of the convexification method is to include some suitable Carleman weight functions into the mismatch cost functionals, making these mismatch functionals uniformly convex. The convexified phenomenon is rigorously proved by employing the well-known Carleman estimates. Several versions of the convexification method [4,29-32,35,38,36,39,51] have been developed since it was first introduced in [34]. Especially, the convexification was successfully tested with experimental data in [27,28,36] for the inverse scattering problem in the frequency domain given only backscattering data. We consider the convexification method as the first generation of numerical methods based on Carleman estimates to solve nonlinear inverse problems. Although effective, the convexification method has a drawback. It is time-consuming. We, therefore, propose to apply the Carleman contraction mapping method, see [48,50,62]. The strength of the Carleman contraction mapping method includes global and fast convergence; i.e., this method can provide reliable numerical solutions without requesting a good initial guess and the rate of the convergence is $O(\theta^n)$ where $\theta \in (0,1)$ and n is the number of iterations. For more details about these strengths, we refer the reader to [62].

The Carleman contraction mapping methods developed in [48,50,62] are suitable for solving nonlinear elliptic equations given Cauchy boundary data. However, the governing equation for Problem 1.1 is hyperbolic. Hence, to place Problem 1.1 into the framework of the Carleman contraction mapping method, we must reduce the time dimension. To achieve this, we express the function $u(\mathbf{x},t)$, for $(\mathbf{x},t) \in \Omega \times (0,T)$, through its Fourier coefficients $u_1(\mathbf{x}), u_2(\mathbf{x}), \dots$, where $\mathbf{x} \in \Omega$. These coefficients are related to the polynomial-exponential basis of $L^2(0,T)$ introduced in [33]. Using straightforward algebra, we derive an approximate model consisting of a system of elliptic PDEs for these Fourier coefficients. As a result, the time dimension is reduced, and the Carleman contraction mapping method can be applied. This process suggests our approach the name: "the time dimensional reduction method." Another benefit of this method is its more efficient computational cost, as we are now dealing with a d dimensional problem instead of a d+1 dimensional one.

The paper is organized as follows. In Section 2, we introduced the time reduction model. In Section 3, we recall a version of the Carleman contraction mapping method and its convergence. In Section 4, we present several numerical results.

2. An approximate model

In this section, we derive a system of nonlinear partial differential equations. The solution to this system directly yields the solution to Problem 1.1. It follows from the initial conditions in (1.1) $u(\mathbf{x}, 0) = f(\mathbf{x})$ and $u_t(\mathbf{x}, 0) = -a(\mathbf{x})f(\mathbf{x})$ that

$$a(\mathbf{x}) = -\frac{u_t(\mathbf{x}, 0)}{u(\mathbf{x}, 0)} \sim -\frac{u_t(\mathbf{x}, 0)u(\mathbf{x}, 0)}{|u(\mathbf{x}, 0)|^2 + \eta^2}, \quad \mathbf{x} \in \Omega$$
(2.1)

for a fixed regularization number $0 < \eta \ll 1$.

Remark 2.1. The replacement of $-\frac{u_t(\mathbf{x},0)}{u(\mathbf{x},0)}$ by its regularized version $-\frac{u_t(\mathbf{x},0)u(\mathbf{x},0)}{|u(\mathbf{x},0)|^2+\eta^2}$ in (2.1) is necessary. This approximation helps prevent a situation where the denominator of the fraction $-\frac{u_t(\mathbf{x},0)}{u(\mathbf{x},0)}$ becomes zero for some values of \mathbf{x} .

Substituting (2.1) into the governing hyperbolic equation in (1.1), we derive the following approximate equation

$$u_{tt}^{\eta}(\mathbf{x},t) - \frac{u_{t}^{\eta}(\mathbf{x},0)u^{\eta}(\mathbf{x},0)}{|u^{\eta}(\mathbf{x},0)|^{2} + \eta^{2}} u_{t}^{\eta}(\mathbf{x},t) - \Delta u^{\eta}(\mathbf{x},t) = 0 \quad (\mathbf{x},t) \in \mathbb{R}^{d} \times (0,T]$$
(2.2)

for an approximation u^n of the wave function u. To address Problem 1.1, we compute the solution for (2.2) given the lateral data of the function u^n on $\partial\Omega \times [0,T]$ as in (1.2) when u^n replaces u. Once we obtain the solution $u^n(\mathbf{x},t)$ for $(\mathbf{x},t)\in\Omega\times[0,T]$ to (2.2), we can set the required function

 $f(\mathbf{x})$ as $u^\eta(\mathbf{x},0)$ for $\mathbf{x} \in \Omega$. However, given that (2.2) is nonlocal and nonlinear, finding its solution is extremely challenging. Currently, an efficient numerical method to handle this task is not yet developed. We only demonstrate a numerical solver for the following approximation where the time variable and the nonlocal terms are eliminated. The first step in removing the time dimension is to cut-off the Fourier series of $u^\eta(\mathbf{x},t)$ with respect to an appropriate basis of $L^2(0,T)$. We choose the polynomial-exponential basis $\{\Psi_n\}_{n\geq 1}$ originally introduced in [33]. The set $\{\Psi_n\}_{n\geq 1}$ is constructed as follows. For any $t\in (0,T)$, we define $\phi_n(t)=t^{n-1}e^t$. It is clear that the set $\{\phi_n\}_{n\geq 1}$ is complete in $L^2(0,T)$. By applying the Gram-Schmidt orthonormalization process to this set, we obtain an orthonormal basis for $L^2(0,T)$, which is denoted by $\{\Psi_n\}_{n\geq 1}$.

Remark 2.2. The polynomial-exponential basis set $\{\Psi_n\}_{n\geq 1}$ was initially introduced in [33] as a tool to solve inverse problems. We have demonstrated its effectiveness by employing to numerous inverse problems of nearly all types of equations. This includes elliptic equations [27–29,49,65], parabolic equations [18,48,50], hyperbolic equations [52,58], transport equations [40], and full radiative transfer equation [74]. In addition, we have used this basis to solve the critical task of differentiating noisy data, as described in [67].

For $(\mathbf{x}, t) \in \Omega \times [0, T]$, we approximate

$$u^{\eta}(\mathbf{x},t) = \sum_{n=1}^{\infty} u_n(\mathbf{x}) \Psi_n(t) \approx \sum_{n=1}^{N} u_n(\mathbf{x}) \Psi_n(t)$$
(2.3)

for some cut-off number N, chosen later in Section 4.2, where

$$u_n(\mathbf{x}) = \int_0^T u^n(\mathbf{x}, t) \Psi_n(t) dt, \quad n \ge 1.$$
(2.4)

Note that in (2.3) and (2.4), rather than writing u_n^{η} , we write u_n and drop the superscript $^{\eta}$ for simplicity. This is acceptable in the context that η is a fixed number. Substituting (2.3) into the governing equation (2.2) gives

$$\sum_{n=1}^{N} u_n(\mathbf{x}) \Psi_n''(t) - \frac{\left[\sum_{l=1}^{N} u_l(\mathbf{x}) \Psi_l'(0)\right] \left[\sum_{l=1}^{N} u_l(\mathbf{x}) \Psi_l(0)\right]}{\left|\sum_{l=1}^{N} u_l(\mathbf{x}) \Psi_l(0)\right|^2 + \eta^2} \sum_{n=1}^{N} u_n(\mathbf{x}) \Psi_n'(t) - \sum_{n=1}^{N} \Delta u_n(\mathbf{x}) \Psi_n(t) = 0$$
(2.5)

for $(\mathbf{x},t) \in \Omega \times (0,T]$. For each $m \in \{1,\ldots,N\}$, multiply $\Psi_m(t)$ to both sides of (2.5) and then integrate the resulting equation. We obtain

$$\sum_{n=1}^{N} u_n(\mathbf{x}) \int_{0}^{T} \Psi_n''(t) \Psi_m(t) dt - \frac{\left[\sum_{l=1}^{N} u_l(\mathbf{x}) \Psi_l'(0)\right] \left[\sum_{l=1}^{N} u_l(\mathbf{x}) \Psi_l(0)\right]}{\left|\sum_{l=1}^{N} u_l(\mathbf{x}) \Psi_l(0)\right|^2 + \eta^2} \sum_{n=1}^{N} u_n(\mathbf{x}) \int_{0}^{T} \Psi_n'(t) \Psi_m(t) dt - \sum_{n=1}^{N} \Delta u_n(\mathbf{x}) \int_{0}^{T} \Psi_n(t) \Psi_m(t) dt = 0$$
(2.6)

for $\mathbf{x} \in \Omega$. Define the vector $U = (u_1, \dots, u_N)^T$. Since $\{\Psi_n\}_{n \ge 1}$ is an orthonormal basis of $L^2(0,T)$, we can deduce from (2.6) that

$$\Delta U(\mathbf{x}) - SU(\mathbf{x}) = F(U(\mathbf{x}))$$
 for all $\mathbf{x} \in \Omega$ (2.7)

where the matrix S is given by

$$S = (s_{mn})_{m,n=1}^{N} = \left(\int_{0}^{1} \Psi_{n}''(t)\Psi_{m}(t)dt\right)_{m,n=1}^{N}$$
(2.8)

and the function $F = [F_1 \quad F_2 \quad \dots \quad F_N]^T : \mathbb{R}^N \to \mathbb{R}^N$ whose the m^{th} component, $m = 1, \dots, N$, is defined as

$$F_{m}(V) = -\frac{\left[\sum_{l=1}^{N} v_{l} \Psi_{l}'(0)\right] \left[\sum_{l=1}^{N} v_{l} \Psi_{l}(0)\right]}{\left|\sum_{l=1}^{N} v_{l} \Psi_{l}(0)\right|^{2} + \eta^{2}} \sum_{n=1}^{N} v_{n} \int_{0}^{T} \Psi_{n}'(t) \Psi_{m}(t) dt$$
(2.9)

for all $V = \begin{bmatrix} v_1 & v_2 & \dots & v_N \end{bmatrix}^T$. Due to (2.3) and the boundedness of $u(\mathbf{x},t)$, see (1.3), the vector U is bounded, say, there is a positive number \mathbf{M} depending only on M, (which is a bound for $|u(\mathbf{x},t)|$, see (1.3)), N, $\{\Psi_n\}_{n=1}^N$ and T such that

$$|U(\mathbf{x})| \le \mathbf{M}$$
 for all $\mathbf{x} \in \Omega$. (2.10)

On the other hand, it follows from (1.2) and (2.4) that

$$U(\mathbf{x}) = \left(\int_{0}^{T} p(\mathbf{x}, t) \Psi_{m}(t) dt\right)_{m=1}^{N}, \text{ and } \partial_{\nu} U(\mathbf{x}) = \left(\int_{0}^{T} q(\mathbf{x}, t) \Psi_{m}(t) dt\right)_{m=1}^{N}$$
(2.11)

for all $\mathbf{x} \in \partial \Omega$. So, we have derived the following "time-reduction" model

$$\begin{cases} \Delta U(\mathbf{x}) - SU(\mathbf{x}) = F(U(\mathbf{x})) & \mathbf{x} \in \Omega \\ U(\mathbf{x}) = \left(\int_0^T p(\mathbf{x}, t) \Psi_m(t) dt \right)_{m=1}^N & \mathbf{x} \in \partial \Omega, \\ \partial_\nu U(\mathbf{x}) = \left(\int_0^T q(\mathbf{x}, t) \Psi_m(t) dt \right)_{m=1}^N & \mathbf{x} \in \partial \Omega. \end{cases}$$
(2.12)

Remark 2.3 (The validity of the approximation model (2.12)). Due to the truncation in (2.3), and the term-by-term differentiation to obtain (2.5), problem (2.12) is not precise. Proving the convergence of this model as $N \to \infty$ is extremely challenging. Since this paper focuses on computation, we do not address this issue here. Instead, we assume that (2.12) well-approximates the model for the Fourier coefficients $U(\mathbf{x}) = (u_1(\mathbf{x}) \dots u_N(\mathbf{x}))^T$ of the function $u(\mathbf{x},t)$. Although the validity of this approximation model is not theoretically proven, we numerically observe its strength. In fact, similar approximations were successfully applied in [27–29,49] in which we solved the highly nonlinear and severely ill-posed inverse scattering problem with backscattering data experimentally measured by microwave facilities built at the University of North Carolina at Charlotte. The successful applications of several versions of this approximation with highly noisy simulated data can be found at [40,52,58,65,74].

Remark 2.4 (The choice of the basis $\{\Psi_n\}_{n\geq 1}$). The use of the basis $\{\Psi_n\}_{n\geq 1}$ is crucial to the efficacy of our method. One may question why we have chosen this specific basis out of countless alternatives for the Fourier expansion in (2.3). The answer lies in the limitations of more common bases like Legendre polynomials or trigonometric functions. These bases typically commence with a constant function, whose derivatives are identically zero. As a result, the corresponding Fourier coefficient $u_1(\mathbf{x})$ in the sums $\sum_{n=1}^N u_n(\mathbf{x})\Psi_n'(t)$ and $\sum_{n=1}^N u_n(\mathbf{x})\Psi_n''(t)$ in (2.5) is overlooked, causing some inaccuracy of the outcome. The basis $\{\Psi_n\}_{n\geq 1}$ is suitable for (2.4) as it fulfills the necessary condition wherein the derivatives of Ψ_n , for $n\geq 1$, are not constantly zero. The effectiveness of this basis is well-documented in various research, such as in [52,67]. In the study [52], we use the basis $\{\Psi_n\}_{n\geq 1}$ and a traditional trigonometric basis to expand wave fields and address problems in photo-acoustic and thermo-acoustic tomography. Our results indicated a notably superior performance from the polynomial-exponential basis. In [67], we employed Fourier expansion to compute the derivatives of data affected by noise. Our findings confirmed that the basis $\{\Psi_n\}_{n\geq 1}$ outperformed the trigonometric basis in terms of accuracy when differentiating term-by-term of the Fourier expansion in solving ill-posed problems.

Remark 2.5. The task of solving Problem 1.1 is reduced to the problem of computing solution to (2.12). In fact, let $U^{\text{comp}} = (u_1^{\text{comp}}, \dots, u_N^{\text{comp}})^T$ denote the computed solution to (2.12). Then, since $f(\mathbf{x}) = u(\mathbf{x}, 0)$ and due to (2.3), we set the desired solution to Problem 1.1 as

$$f^{\text{comp}}(\mathbf{x}) = \sum_{n=1}^{N} u_n^{\text{comp}}(\mathbf{x}) \Psi_n(0) \quad \text{for } \mathbf{x} \in \Omega.$$
 (2.13)

We present the Carleman contraction method to solve (2.12) in the next section. Some earlier versions of this method can be found in [48,50,62].

3. The Carleman contraction method

Some versions of the Carleman contraction method, which were established in [48,50,62], and the one in this paper rely on Carleman estimates. We recall a version of Carleman estimate.

Lemma 3.1 (Carleman estimate). Fix a point $\mathbf{x}_0 \in \mathbb{R}^d \setminus \Omega$. Define $r(\mathbf{x}) = |\mathbf{x} - \mathbf{x}_0|$ for all $\mathbf{x} \in \Omega$. Let $b > \max_{\mathbf{x} \in \overline{\Omega}} r(\mathbf{x})$ be a fixed constant. There exist positive constants β depending only on \mathbf{x}_0 , Ω , b, and d such that for all function $v \in C^2(\overline{\Omega})$ satisfying

$$v(\mathbf{x}) = \partial_v v(\mathbf{x}) = 0$$
 for all $\mathbf{x} \in \partial \Omega$, (3.1)

the following estimate holds true

$$\int_{\Omega} e^{2\lambda r^{-\beta}(\mathbf{x})} |\Delta v|^2 d\mathbf{x} \ge C\lambda \int_{\Omega} e^{2\lambda r^{-\beta}(\mathbf{x})} |\nabla v(\mathbf{x})|^2 d\mathbf{x} + C\lambda^3 \int_{\Omega} e^{2\lambda r^{-\beta}(\mathbf{x})} |v(\mathbf{x})|^2 d\mathbf{x}$$
(3.2)

for all $\lambda \ge \lambda_0$. Here, $\lambda_0 = \lambda_0(\mathbf{x}_0, \Omega, d, \beta, b)$ and $C = C(\mathbf{x}_0, \Omega, d, \beta, b) > 0$ depend only on the listed parameters.

Lemma 3.1 can be straightforwardly derived from [59, Lemma 5]. For a detailed exposition of the proof, we direct the reader to [53, Lemma 2.1]. Another approach to derive (3.2), using a different Carleman weight function, involves the application of the Carleman estimate from [47, Chapter 4, Section 1, Lemma 3] for generic parabolic operators. The methodology to derive (3.2) via [47, Chapter 4, Section 1, Lemma 3] resembles the one in [52, Section 3], albeit with the Laplacian swapped out for the operator $\text{Div}(A\nabla \cdot)$. We would like to specifically highlight to the reader the varied forms of Carleman estimates for all three types of differential operators (elliptic, parabolic, and hyperbolic) and their respective applications in inverse problems and computational mathematics [5,7,37,60]. Additionally, it is noteworthy that certain Carleman estimates remain valid for all functions v that satisfy $v|_{\partial\Omega} = 0$ and $\partial_v v|_{\Gamma} = 0$, where Γ constitutes a portion of $\partial\Omega$. Examples can be seen in [41,64]. These Carleman estimates are applicable to the resolution of quasilinear elliptic PDEs given the data on only a part of $\partial\Omega$.

We will seek the solution U to (2.12) in the set of admissible solutions

$$H = \left\{ h \in H^{s}(\Omega)^{N} : \|h\|_{H^{s}(\Omega)^{N}} \le \mathbf{M}, h|_{\partial\Omega} = \left(\int_{0}^{T} p(\mathbf{x}, t) \Psi_{m}(t) dt \right)_{m=1}^{N} \text{ and } \partial_{\nu} h|_{\partial\Omega} = \left(\int_{0}^{T} q(\mathbf{x}, t) \Psi_{m}(t) dt \right)_{m=1}^{N} \right\}$$

$$(3.3)$$

where s is an integer with $s > \lceil d/2 \rceil + 2$. Throughout the paper, we assume that H is nonempty. Let λ_0 be the number in Lemma 3.1. For $\lambda \ge \lambda_0$, we define the map $\Phi_{\lambda,\varepsilon}: H \to H$

$$\Phi_{\lambda,\epsilon}(V) = \min_{\varphi \in H} \int_{\Omega} e^{2\lambda r^{-\beta}(\mathbf{x})} \left| \Delta \varphi - S\varphi - F(V(\mathbf{x})) \right|^2 d\mathbf{x} + \epsilon \|\varphi\|_{H^s(\Omega)^N}^2$$
(3.4)

where $\epsilon > 0$ is a regularization parameter. The map $\Phi_{\lambda,\epsilon}$ is well-defined. In fact, for each $V \in H$, the functional

$$J_{\lambda,\epsilon}(V): H \to \mathbb{R}, \quad \varphi \mapsto \int_{\Omega} e^{2\lambda r^{-\beta}(\mathbf{x})} \left| \Delta \varphi - S \varphi - F(V(\mathbf{x})) \right|^2 d\mathbf{x} + \epsilon \|\varphi\|_{H^{s}(\Omega)^{N}}^{2}$$
(3.5)

is strictly convex. It has a unique minimizer on a closed and convex subset H of $H^s(\Omega)^N$. We refer the reader to [62, Remark 3.1] for more details. A similar argument for the well-posedness of the map $\Phi_{\lambda,\varepsilon}$ can be found in [48, Theorem 4.1].

Remark 3.1 (The Carleman quasi-reversibility method). Consider a vector-valued function V in H. Define φ as $\Phi_{\lambda,\varepsilon}(V)$. As $\varphi \in H$ minimizes the function $J_{\lambda,\varepsilon}(V)$, it can be informally said that computing φ is about finding a solution for the following system of equations:

$$\begin{cases} \Delta \varphi - S\varphi - F(V(\mathbf{x})) = 0 & \mathbf{x} \in \Omega, \\ \varphi(\mathbf{x}) = \left(\int_0^T p(\mathbf{x}, t) \Psi_m(t) dt \right)_{m=1}^N & \mathbf{x} \in \partial \Omega, \\ \partial_{\nu} \varphi(\mathbf{x}) = \left(\int_0^T q(\mathbf{x}, t) \Psi_m(t) dt \right)_{m=1}^N & \mathbf{x} \in \partial \Omega. \end{cases}$$
(3.6)

Due to the presence of the regularization term $\epsilon \|\varphi\|_{H^{s}(\Omega)}^2$, we refer to φ as the regularized solution of problem (3.6). The technique for determining the regularized solution to the linear equation (3.6) by minimizing $J_{\lambda,\epsilon}(V)$ is named the Carleman quasi-reversibility method. The name of this method is suggested by the existence of the Carleman weight function in the formulation of $J_{\lambda,\epsilon}(V)$, as well as the use of the quasi-reversibility technique to address linear PDEs with Cauchy data. We refer the reader to [46] for original work regarding the quasi-reversibility method.

Let p^* and q^* be the noiseless versions of the measured data p and q respectively. We assume that these data are corrupted by noise with the noise level δ . Define the set

$$E = \left\{ \mathbf{e} \in H^s(\Omega)^N : \mathbf{e}|_{\partial\Omega} = p - p^* \text{ and } \partial_{\nu} \mathbf{e}|_{\partial\Omega} = q - q^* \right\}$$

By noise level δ , we mean that $E \neq \emptyset$ and

$$\inf\{\|\mathbf{e}\|_{H_{S}(\Omega)N} : \mathbf{e} \in E\} < \delta. \tag{3.7}$$

By (3.7), there is a vector function $\mathbf{e} \in H^s(\Omega)^N$ such that

$$\begin{cases}
\|\mathbf{e}\|_{H^{s}(\Omega)^{N}} < 2\delta, \\
\mathbf{e}|_{\partial\Omega} = p - p^{*}, \\
\partial_{\nu}\mathbf{e}|_{\partial\Omega} = q - q^{*}.
\end{cases}$$
(3.8)

Remark 3.2. The condition that $E \neq \emptyset$ and (3.7), as well as, (3.8) imply that the differences $p - p^*$ and $q - q^*$ are traces of smooth vector-valued functions on $\partial\Omega$. This implies the noise must exhibit smooth characteristics, which may not always be true in real-world scenarios. The demand for smoothness is a crucial component in the convergence result in Theorem 3.1. In real-world applications, the data can be smoothed using several established techniques, such as spline curves or the Tikhonov regularization approach. Nevertheless, this smoothing step can be relaxed during numerical investigations. This implies that our method's practical application may surpass its theoretical proof. In our numerical tests, we do not have to smooth out the noisy data. Instead, we directly derive the desired numerical solutions to (1.1) using the noisy (raw) data of the form

$$p = p^*(1 + \delta \text{rand})$$
 and $q = q^*(1 + \delta \text{rand})$ (3.9)

where rand is a function taking uniformly distributed random numbers in the range [-1,1].

Let U^* be the true solution to the following analog of (2.12), in which the boundary data are replaced by the exact ones,

$$\begin{cases} \Delta U^*(\mathbf{x}) - SU^*(\mathbf{x}) = F(U^*(\mathbf{x})) & \mathbf{x} \in \Omega \\ U(\mathbf{x}) = \left(\int_0^T p^*(\mathbf{x}, t) \Psi_m(t) dt \right)_{m=1}^N & \mathbf{x} \in \partial \Omega, \\ \partial_\nu U(\mathbf{x}) = \left(\int_0^T q^*(\mathbf{x}, t) \Psi_m(t) dt \right)_{m=1}^N & \mathbf{x} \in \partial \Omega. \end{cases}$$
(3.10)

Define the sequence

$$\begin{cases} U_0 \text{ is an arbitrary vector-valued function in } H, \\ U_{n+1} = \Phi_{\lambda,\varepsilon}(U_n), \quad n \geq 0. \end{cases}$$
 (3.11)

We claim that $\{U_n\}_{n\geq 1}$ well-approximates U^* with respect to the Carleman weighted norm

$$\|\varphi\|_{\lambda,\epsilon} = \left(\int\limits_{\Omega} e^{2\lambda r^{-\beta}(\mathbf{x})} (|\varphi|^2 + |\nabla \varphi|^2) d\mathbf{x}\right)^{1/2} + \frac{\epsilon}{\lambda} \|\varphi\|_{H^{3}(\Omega)^{N}}$$
(3.12)

for all $\varphi \in H^s(\Omega)^N$, for $\epsilon > 0$ and $\lambda > \lambda_0$.

We have the theorem.

Theorem 3.1. Recall β and λ_0 as in Lemma 3.1. Let $\lambda \geq \lambda_0$ be such that (3.2) holds true. Let $\{U_n\}_{n\geq 0} \subset H$ be the sequence defined in (3.11). Assume that (3.10) has a unique solution U^* with $\|U^*\|_{H^s(\Omega)^N} < \mathbf{M} - 2\delta$. Let λ_0 be the number in Lemma 3.1. Then, for all $\lambda \geq \lambda_0$,

$$||U_{n+1} - U^*||_{\lambda,\epsilon}^2 \le \left(\frac{C}{\lambda}\right)^{n+1} ||U_0 - U^*||_{\lambda,\epsilon}^2 + C||\mathbf{e}||_{\lambda,\epsilon}^2 + \frac{C/\lambda}{1 - C/\lambda} \left(\int\limits_{\Omega} e^{2\lambda r^{-\beta}(\mathbf{x})} |\Delta \mathbf{e}|^2 d\mathbf{x} + \int\limits_{\Omega} |\mathbf{e}|^2 d\mathbf{x} + \epsilon ||\mathbf{e}||_{H^s(\Omega)^N}^2 + \epsilon ||U^*||_{H^s(\Omega)^N}^2\right)$$
(3.13)

where C is a positive constant depending only on \mathbf{x}_0 , Ω , β , T, $\{\Psi_n\}_{n=1}^N$, M, η and d.

Theorem 3.1 has a broader scope than the theorem presented in [62, Theorem 4.1] in the sense that Theorem 3.1 can be applied to solve systems, whereas [62, Theorem 4.1] pertains to a single equation. Two simpler versions of this convergence theorem for the case of exact data can be found in [48,50]. On the other hand, the proof of the convergence in [48,50,62] requires the globally Lipschitz property of F while the vector-valued function F in this work is only locally Lipschitz.

Remark 3.3. Estimate (3.13) is interesting in the sense that it, together with (3.8), guarantees that U_n tends to U^* as the noise level δ and the regularization parameter ϵ tends to 0. In particular, fix $\lambda \gg 1$ and set $\epsilon = O(\delta^2)$, the convergence rate is Lipschitz.

Proof of Theorem 3.1. Since the function F is smooth, it is Lipschitz in the bounded domain H. In other words, we can find a constant $C_{F,\mathbf{M}}$ depending on F and \mathbf{M} such that

$$|F(V_1(\mathbf{x})) - F(V_2(\mathbf{x}))| \le C_{FM}|V_1(\mathbf{x}) - V_2(\mathbf{x})| \quad \text{for all } \mathbf{x} \in \overline{\Omega}$$

$$(3.14)$$

for all V_1, V_2 in H. Here, we have used the fact that when V_1 and V_2 are in H, $|V_1(\mathbf{x})| \leq C\mathbf{M}$ and $|V_1(\mathbf{x})| \leq C\mathbf{M}$ for all $\mathbf{x} \in \Omega$ where C > 0 is the embedding constant for $H^s(\Omega) \to L^\infty(\Omega)$. It follows from (3.8) and the assumption $||U^*||_{H^s(\Omega)^N} < \mathbf{M} - 2\delta$ that $||U^* + \mathbf{e}||_{H^s(\Omega)^N} \leq \mathbf{M}$. Hence, $U^* + \mathbf{e}$ is in H. Fix $n \geq 0$. Since H is a convex subset of $H^s(\Omega)^N$, the vector-valued function $U_{n+1} + \tau(U^* + \mathbf{e} - U_{n+1})$ is in H for all $\tau \in (0,1)$. Since U_{n+1} is the minimizer of $J_{\lambda,\varepsilon}(U_n)$ in H, we have

$$\frac{J_{\lambda,\epsilon}(U_n)(U_{n+1} + \tau(U^* + \mathbf{e} - U_{n+1})) - J_{\lambda,\epsilon}(U_n)(U_{n+1})}{\tau} \ge 0 \quad \text{for all } \tau \in (0,1). \tag{3.15}$$

It follows from (3.5) and (3.15) that

$$\frac{1}{\tau} \int\limits_{\Omega} e^{2\lambda r^{-\beta}(\mathbf{x})} [\Delta (2U_{n+1} + \tau(U^* + \mathbf{e} - U_{n+1})) - S(2U_{n+1} + \tau(U^* + \mathbf{e} - U_{n+1})) + 2F(U_n(\mathbf{x}))]$$

$$\times [\Delta(\tau(U^* + \mathbf{e} - U_{n+1})) - S(\tau(U^* + \mathbf{e} - U_{n+1}))] d\mathbf{x}$$

$$+ \epsilon \langle 2U_{n+1} + \tau(U^* + \mathbf{e} - U_{n+1}), \tau(U^* + \mathbf{e} - U_{n+1}) \rangle_{H^s(\Omega)^N} \ge 0.$$

Letting τ tend to 0^+ , we obtain

$$\left\langle e^{2\lambda r^{-\beta}(\mathbf{x})} [\Delta U_{n+1} - SU_{n+1} - F(U_n(\mathbf{x}))], \Delta(U^* + \mathbf{e} - U_{n+1}) - S(U^* + \mathbf{e} - U_{n+1}) \right\rangle_{L^2(\Omega)^N} + \epsilon \langle U_{n+1}, U^* + \mathbf{e} - U_{n+1} \rangle_{H^s(\Omega)^N} \ge 0. \tag{3.16}$$

On the other hand, since U^* satisfies (3.10),

$$\left\langle e^{2\lambda r^{-\beta}(\mathbf{x})} [\Delta U^* - SU^* - F(U^*(\mathbf{x}))], \Delta (U^* + \mathbf{e} - U_{n+1}) - S(U^* + \mathbf{e} - U_{n+1}) \right\rangle_{L^2(\Omega)^N} \\ + \epsilon \left\langle U^*, U^* + \mathbf{e} - U_{n+1} \right\rangle_{H^s(\Omega)^N} = \epsilon \left\langle U^*, U^* + \mathbf{e} - U_{n+1} \right\rangle_{H^s(\Omega)^N}.$$
 (3.17)

It follows from (3.16) and (3.17) that

$$\begin{split} \left\langle e^{2\lambda r^{-\beta}(\mathbf{x})} [\Delta(U_{n+1} - U^*) - S(U_{n+1} - U^*) - F(U_n(\mathbf{x})) + F(U^*(\mathbf{x}))], \\ \Delta(U^* + \mathbf{e} - U_{n+1}) - S(U^* + \mathbf{e} - U_{n+1}) \right\rangle_{L^2(\Omega)^N} \\ + \varepsilon \langle U_{n+1} - U^*, U^* + \mathbf{e} - U_{n+1} \rangle_{H^3(\Omega)^N} \geq -\varepsilon \langle U^*, U^* + \mathbf{e} - U_{n+1} \rangle_{H^3(\Omega)^N}, \end{split}$$

which implies

$$\left\langle e^{2\lambda r^{-\beta}(\mathbf{x})} [\Delta(U_{n+1} - U^* - \mathbf{e}) - S(U_{n+1} - U^* - \mathbf{e}) - F(U_n(\mathbf{x})) + F(U^*(\mathbf{x}))], \right.$$

$$\left. \Delta(U_{n+1} - U^* - \mathbf{e}) - S(U_{n+1} - U^* - \mathbf{e}) \right\rangle_{L^2(\Omega)^N}$$

$$+ \left\langle e^{2\lambda r^{-\beta}(\mathbf{x})} [\Delta \mathbf{e} - S\mathbf{e} - F(U_n(\mathbf{x})) + F(U^*(\mathbf{x}))], \Delta(U_{n+1} - U^* - \mathbf{e}) - S(U_{n+1} - U^* - \mathbf{e}) \right\rangle_{L^2(\Omega)^N}$$

$$+ \epsilon \langle U_{n+1} - U^* - \mathbf{e}, U_{n+1} - U^* - \mathbf{e} \rangle_{H^s(\Omega)^N} \le -\epsilon \langle U^*, U_{n+1} - U^* - \mathbf{e} \rangle_{H^s(\Omega)^N}.$$
 (3.18)

Define $h_n = U_n - U^* - \mathbf{e}$ for $n \ge 0$. Using the inequality $2ab \le \frac{a^2}{8} + 8b^2$, we have

$$\begin{split} \int\limits_{\Omega} e^{2\lambda r^{-\beta}(\mathbf{x})} |\Delta h_{n+1} - Sh_{n+1}|^2 d\mathbf{x} + \epsilon \|h\|_{H^s(\Omega)^N}^2 &\leq C \bigg[\int\limits_{\Omega} e^{2\lambda r^{-\beta}(\mathbf{x})} |F(U_n(\mathbf{x})) - F(U^*(\mathbf{x}))|^2 d\mathbf{x} \\ &+ \int\limits_{\Omega} e^{2\lambda r^{-\beta}(\mathbf{x})} |\Delta \mathbf{e} - S\mathbf{e}|^2 d\mathbf{x} + \epsilon \|\mathbf{e}\|_{H^s(\Omega)^N}^2 + \epsilon \|U^*\|_{H^s(\Omega)^N}^2 \bigg]. \end{split} \tag{3.19}$$

From this point forward, C denotes the substantial constants that are determined solely by F, M, Ω , x_0 , b, β , N, $\{\Psi\}_{n=1}^N$, and d. Note that the value of C may vary across different estimates. We next use (3.14) and apply the inequality $(a-b)^2 \ge \frac{a^2}{2} - b^2$ to obtain from (3.19) that

$$\int_{\Omega} e^{2\lambda r^{-\beta}(\mathbf{x})} |\Delta h_{n+1}|^{2} d\mathbf{x} + \epsilon ||h_{n+1}||_{H^{s}(\Omega)^{N}}^{2} \leq C \left[\int_{\Omega} e^{2\lambda r^{-\beta}(\mathbf{x})} |Sh_{n+1}|^{2} d\mathbf{x} + \int_{\Omega} e^{2\lambda r^{-\beta}(\mathbf{x})} |U_{n}(\mathbf{x}) - U^{*}(\mathbf{x})|^{2} d\mathbf{x} + \int_{\Omega} e^{2\lambda r^{-\beta}(\mathbf{x})} |\Delta \mathbf{e} - S\mathbf{e}|^{2} d\mathbf{x} + \epsilon ||\mathbf{e}||_{H^{s}(\Omega)^{N}}^{2} + \epsilon ||U^{*}||_{H^{s}(\Omega)^{N}}^{2} \right].$$
(3.20)

Let λ_0 be the number in Lemma 3.1. Using the Carleman estimate (3.2) for each component of h_{n+1} , we have for all $\lambda \geq \lambda_0$

$$\int_{\Omega} e^{2\lambda r^{-\beta}(\mathbf{x})} |\Delta h_{n+1}|^2 d\mathbf{x} \ge C\lambda \int_{\Omega} e^{2\lambda r^{-\beta}(\mathbf{x})} |\nabla h_{n+1}(\mathbf{x})|^2 d\mathbf{x} + C\lambda^3 \int_{\Omega} e^{2\lambda r^{-\beta}(\mathbf{x})} |h_{n+1}(\mathbf{x})|^2 d\mathbf{x}. \tag{3.21}$$

Combining (3.20) and (3.21), recalling that $h_n = U_n - U^* - \mathbf{e}$, and noting that $\lambda \gg 1$ give

$$\lambda \int_{\Omega} e^{2\lambda r^{-\beta}(\mathbf{x})} [|h_{n+1}(\mathbf{x})|^{2} + |\nabla h_{n+1}(\mathbf{x})|^{2} d\mathbf{x} + \epsilon ||h_{n+1}||_{H^{s}(\Omega)^{N}}^{2}$$

$$\leq C \Big[\int_{\Omega} e^{2\lambda r^{-\beta}(\mathbf{x})} |h_{n}|^{2} d\mathbf{x} + \int_{\Omega} e^{2\lambda r^{-\beta}(\mathbf{x})} |\Delta \mathbf{e}|^{2} d\mathbf{x} + \int_{\Omega} |\mathbf{e}|^{2} d\mathbf{x} + \epsilon ||\mathbf{e}||_{H^{s}(\Omega)^{N}}^{2} + \epsilon ||U^{*}||_{H^{s}(\Omega)^{N}}^{2} \Big]$$

$$\leq C \Big[\int_{\Omega} e^{2\lambda r^{-\beta}(\mathbf{x})} [|h_{n}|^{2} + |\nabla h_{n}|^{2}] d\mathbf{x} + \frac{\epsilon}{\lambda} ||h_{n}||_{H^{s}(\Omega)^{N}}^{2} + \int_{\Omega} e^{2\lambda r^{-\beta}(\mathbf{x})} |\Delta \mathbf{e}|^{2} d\mathbf{x} + \int_{\Omega} |\mathbf{e}|^{2} d\mathbf{x} + \epsilon ||\mathbf{e}||_{H^{s}(\Omega)^{N}}^{2} + \epsilon ||U^{*}||_{H^{s}(\Omega)^{N}}^{2} \Big]. \tag{3.22}$$

It follows from (3.12) and (3.22) that

$$\|h_{n+1}\|_{\lambda,\epsilon}^2 \le \frac{C}{\lambda} \Big[\|h_n\|_{\lambda,\epsilon}^2 + \int\limits_{\Omega} e^{2\lambda r^{-\beta}(\mathbf{x})} |\Delta \mathbf{e}|^2 d\mathbf{x} + \int\limits_{\Omega} |\mathbf{e}|^2 d\mathbf{x} + \epsilon \|\mathbf{e}\|_{H^s(\Omega)^N}^2 + \epsilon \|U^*\|_{H^s(\Omega)^N}^2 \Big]. \tag{3.23}$$

Replacing n + 1 by n in (3.23) and then combining the resulting inequality with (3.23) give

$$\|h_{n+1}\|_{\lambda,\epsilon}^{2} \leq \frac{C}{\lambda} \left[\frac{C}{\lambda} \left(\|h_{n-1}\|_{\lambda,\epsilon}^{2} + \int_{\Omega} e^{2\lambda r^{-\beta}(\mathbf{x})} |\Delta \mathbf{e}|^{2} d\mathbf{x} + \int_{\Omega} |\mathbf{e}|^{2} d\mathbf{x} + \epsilon \|\mathbf{e}\|_{H^{s}(\Omega)^{N}}^{2} + \epsilon \|U^{*}\|_{H^{s}(\Omega)^{N}}^{2} \right) + \int_{\Omega} e^{2\lambda r^{-\beta}(\mathbf{x})} |\Delta \mathbf{e}|^{2} d\mathbf{x} + \int_{\Omega} |\mathbf{e}|^{2} d\mathbf{x} + \epsilon \|\mathbf{e}\|_{H^{s}(\Omega)^{N}}^{2} + \epsilon \|U^{*}\|_{H^{s}(\Omega)^{N}}^{2} \right].$$
(3.24)

Continuing the procedure, we obtain

$$\begin{split} \|h_{n+1}\|_{\lambda,\epsilon}^2 &\leq \left(\frac{C}{\lambda}\right)^{n+1} \|h_0\|_{\lambda,\epsilon}^2 + \sum_{i=1}^n \left(\frac{C}{\lambda}\right)^i \left(\int\limits_{\Omega} e^{2\lambda r^{-\beta}(\mathbf{x})} |\Delta \mathbf{e}|^2 d\mathbf{x} + \int\limits_{\Omega} |\mathbf{e}|^2 d\mathbf{x} + \epsilon \|\mathbf{e}\|_{H^s(\Omega)^N}^2 + \epsilon \|U^*\|_{H^s(\Omega)^N}^2\right) \\ &\leq \left(\frac{C}{\lambda}\right)^{n+1} \|h_0\|_{\lambda,\epsilon}^2 + \frac{C/\lambda}{1 - C/\lambda} \left(\int\limits_{\Omega} e^{2\lambda r^{-\beta}(\mathbf{x})} |\Delta \mathbf{e}|^2 d\mathbf{x} + \int\limits_{\Omega} |\mathbf{e}|^2 d\mathbf{x} + \epsilon \|\mathbf{e}\|_{H^s(\Omega)^N}^2 + \epsilon \|U^*\|_{H^s(\Omega)^N}^2\right). \end{split}$$

Using the usual triangle inequality, we obtain (3.13).

Remark 3.4. The name "Carleman contraction" for our approach is inspired by several factors. First, the definition of the sequence $\{U_n\}_{n\geq 0}$ was inspired by the proof of the classical contraction principle. Second, we include a Carleman weight function in the definition of $\Phi_{\lambda,\varepsilon}$. Third, we apply a Carleman estimate in the proof of Theorem 3.1. Furthermore, as demonstrated by estimate (3.23) in the proof, each successive term U_{n+1} moves closer to the actual solution U^* compared to its predecessor U_n . This indicates that the function $\Phi_{\lambda,\varepsilon}$ acts as a contraction towards U^* , independent of the initial choice of U_0 .

4. Numerical study

It is suggested by Remark 2.5 and Theorem 3.1 a Carleman contraction method to solve Problem 1.1. We present this method in Algorithm 1. In this section, we display several numerical examples in 2D computed by Algorithm 1. In all tests below, we set $\Omega = (-1, 1)^2$ and T = 1.

4.1. Discretization and data simulation

To generate noisy data p and q for Problem 1.1, we need to solve the hyperbolic equation (1.1). However, computing the solution to (1.1) on the whole domain $\mathbb{R}^2 \times (0,T)$ is complicated. For simplicity, we replace \mathbb{R}^d with the domain $G = (-3,3)^2$ that contains the computational domain Ω . On G, we arrange a uniform grid of points

$$G = \{\mathbf{x}_{i,j} = (x_i = -1 + (i-1)d_{\mathbf{x}}, y_j = -1 + (j-1)d_{\mathbf{x}}) : 1 \le i, j \le N_{\mathbf{x}}\}$$

$$(4.1)$$

where $N_{\rm x}=241$ and $d_{\rm x}=\frac{2}{N_{\rm y}-1}=.025$. We discretize the time domain (0,T) by the partition

$$\mathcal{T} = \{t_l = (l-1)d_t : 1 \le l \le N_t\}$$

Algorithm 1 The procedure to compute the numerical solution to (1.1).

- 1: Choose a cut-off number N.
- 2: Choose Carleman parameters \mathbf{x}_0 , β , and λ and a regularization parameter ϵ .
- 3: Set n = 0. Choose an arbitrary initial solution $U_0 \in H$.
- 4: Compute $U_{n+1} = \Phi_{\lambda,\epsilon}(U_n)$ where $\Phi_{\lambda,\epsilon}$ is defined in (3.4).
- 5: if $\|U_{n+1}-U_n\|_{L^2(\Omega)} > \kappa_0$ (for some fixed number $\kappa_0>0$) then
- 6: Replace n by n + 1.
- 7: Go back to Step 4.
- 8: else
- 9: Set the computed solution $U^{\text{comp}} = U_{n+1}$.
- 10: end if
- 11: Write $U^{\text{comp}} = (u_1^{\text{comp}}, \dots, u_N^{\text{comp}})^T$ and set the desired solution as in (2.13).

where $N_t = 201$ and $d_t = T/(N_t - 1) = 0.005$.

We write the governing partial differential equation in the finite difference scheme as

$$\frac{u(\mathbf{x}_{ij}, t_{l+1}) - 2u(\mathbf{x}_{ij}, t_l) + u(\mathbf{x}_{ij}, t_{l-1})}{d_t^2} + a(\mathbf{x}_{ij}) \frac{u(\mathbf{x}_{ij}, t_{l+1}) - u(\mathbf{x}_{ij}, t_l)}{d_t} = \Delta^{d_{\mathbf{x}}} u(\mathbf{x}_{ij}, t_l), \tag{4.2}$$

for all $\mathbf{x}_{ij} \in \mathcal{G}$ and $t_l \in \mathcal{T}$ where

$$\Delta^{d_{\mathbf{X}}} u(\mathbf{x}_{ij}, t_l) = \frac{u(\mathbf{x}_{(i+1)j}, t_l) + u(\mathbf{x}_{(i-1)j}, t_l) + u(\mathbf{x}_{i(j-1)}, t_l) + u(\mathbf{x}_{i(j+1)}, t_l) - 4u(\mathbf{x}_{ij}, t_l)}{d_{\mathbf{x}}^2}.$$

Solving (4.2) for $u(\mathbf{x}_{ij}, t_{l+1})$ gives

$$u(\mathbf{x}_{ij}, t_{l+1}) = \frac{\frac{1}{d_l^2} (2u(\mathbf{x}_{ij}, t_l) - u(\mathbf{x}_{ij}, t_{l-1})) + \frac{a(\mathbf{x}_{ij})}{d_l} u(\mathbf{x}_{ij}, t_l) + \Delta^{d_{\mathbf{x}}} u(\mathbf{x}_{ij}, t_l)}{\frac{1}{d_l^2} + \frac{a(\mathbf{x}_{ij})}{d_l^2}}$$

$$(4.3)$$

for all $\mathbf{x}_{ij} \in \mathcal{G}$ and $t_l \in \mathcal{T}$. Due to the initial conditions in (1.1), we can compute

$$u(\mathbf{x}_{ij}, t_1) = f(\mathbf{x}_{ij}), \quad u(\mathbf{x}_{ij}, t_2) = f(\mathbf{x}_{ij}) - a(\mathbf{x}_{ij})f(\mathbf{x}_{ij})d_t$$

for all $\mathbf{x}_{ij} \in \mathcal{G}$. Using (4.3), we can compute $u(\mathbf{x}_{ij},t_3), u(\mathbf{x}_{ij},t_4), \ldots$, for all $\mathbf{x}_{ij} \in \mathcal{G}$. This method of solving hyperbolic equations is well-known as the explicit method. Having the function u on $\mathcal{G} \times \mathcal{T}$ in hand, we can extract the noiseless data p^* and q^* on $(\mathcal{G} \cap \partial \Omega) \times \mathcal{T}$ easily. The corresponding noisy data p^{δ} and q^{δ} are computed as in (3.9). In our computation, we take $\delta = 0.1$.

4.2. Implementation

We now present some remarkable points in computing solutions to the inverse problem. The first step is to find a suitable number N for (2.3). We employ the strategy in [18] to determine the cut-off number N in step 1. More precisely, the knowledge of given data $p(\mathbf{x},t)$, $(\mathbf{x},t) \in \partial \Omega \times (0,T)$ is helpful in determining the cut-off numbers for step 1 of Algorithm 1. The procedure is based on a trial-and-error process. Inspired by (2.3) and the fact that $u(\mathbf{x},t) = p(\mathbf{x},t)$ for all $(\mathbf{x},t) \in \partial \Omega \times (0,T)$, for each $N \geq 1$, we define the function $\varphi : \mathbb{N} \to \mathbb{R}$ that represents the relative distance between the data p and the truncation of its Fourier expansion in (2.3). The function η is defined as follows

$$\varphi(N) = \frac{\|p(\mathbf{x}) - \sum_{n=1}^{N} p_n(\mathbf{x}) \Psi_n(t)\|_{L^{\infty}(\partial\Omega \times (0,T))}}{\|p(\mathbf{x})\|_{L^{\infty}(\partial\Omega \times (0,T))}} \quad \text{where} \quad p_n(\mathbf{x}) = \int_0^T p(\mathbf{x}, t) \Psi_n(t) dt$$

$$(4.4)$$

We increase the numbers N until $\eta(N)$ is sufficiently small. In our numerical tests below, N=35.

The selection of artificial parameters in Step 2 of Algorithm 1 is facilitated by a process of trial and error. We use a reference test (Test 1 below) where the correct solution is already known. Manually, we select \mathbf{x}_0 , λ , λ , ϵ , κ_0 such that the solution computed through Algorithm 1 is satisfactory. Then, we take these parameters for all other tests where the true solutions are not known. In our computation, $\mathbf{x}_0 = (0, 5.5)$, $\beta = 25$, and $\lambda = 45$. The regularization parameter ϵ is 10^{-5} . We also set the number η in (2.1) is 10^{-11} .

Step 3 of Algorithm 1 requires us to choose a vector-valued function U_0 in H. A straightforward approach for computing such a function involves solving the linear problem, which results from excluding the nonlinearity F from (2.12), namely,

$$\begin{cases} \Delta U_0(\mathbf{x}) - SU_0(\mathbf{x}) = 0 & \mathbf{x} \in \Omega, \\ U_0(\mathbf{x}) = \left(\int_0^T p(\mathbf{x}, t) \Psi_m(t) dt \right)_{m=1}^N & \mathbf{x} \in \partial \Omega, \\ \partial_{\nu} U_0(\mathbf{x}) = \left(\int_0^T q(\mathbf{x}, t) \Psi_m(t) dt \right)_{m=1}^N & \mathbf{x} \in \partial \Omega, \end{cases}$$

$$(4.5)$$

using the Carleman quasi-reversibility method, as indicated in Remark 3.1. Similarly, in Step 4, we aim to minimize $J_{\lambda,\epsilon}(U_n)$ in H, $n \ge 0$. As in Remark 3.1, the minimizer we obtain, U_{n+1} , can be viewed as the regularized solution to the following system

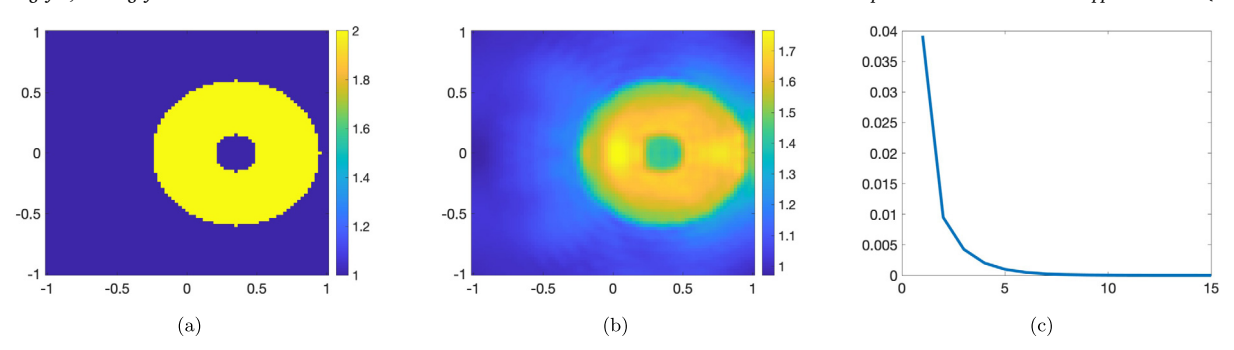


Fig. 1. (a) and (b) the true and computed initial condition f^{true} and f^{comp} respectively; (c) the consecutive relative difference $\frac{\|U_{n+1}-U_n\|_{L^{\infty}(\Omega)}}{\|U_n\|_{L^{\infty}(\Omega)}}$. The horizontal axis of this figure is the number of iteration n. The boundary data used to reconstruct the function f is corrupted with $\delta = 0.1$.

$$\begin{cases} \Delta U_{n+1}(\mathbf{x}) - SU_{n+1} + F(U_n(\mathbf{x})) = 0 & \mathbf{x} \in \Omega, \\ U_{n+1}(\mathbf{x}) = \left(\int_0^T p(\mathbf{x}, t) \Psi_m(t) dt \right)_{m=1}^N & \mathbf{x} \in \partial \Omega, \\ \partial_{\nu} U_{n+1}(\mathbf{x}) = \left(\int_0^T q(\mathbf{x}, t) \Psi_m(t) dt \right)_{m=1}^N & \mathbf{x} \in \partial \Omega. \end{cases}$$

$$(4.6)$$

We briefly mention the numerical implementation of this step. For fixed n, when solving (4.6), we are in the context that U_n and hence the term $F(U_n)$ are known. So, (4.6) is a linear system for U_{n+1} . To compute $U_{n+1}(\mathbf{x})$ in the finite difference scheme, we arrange a grid of points \mathbf{x}_{ij} of $\overline{\Omega}$ in the same manner of (4.1) with Ω replacing G, named as \mathfrak{G} . Then, we can rewrite the differential equations in (4.6) as a linear system $\mathfrak{L}_{n+1} = \mathfrak{F}$ where \mathfrak{U}_{n+1} and \mathfrak{F} are vectors whose entries are $U_{n+1}(\mathbf{x}_{ij})$ and $F(U_n(\mathbf{x}_{ij}))$ respectively. Similarly, we also approximate the Dirichlet and Neumann conditions in (4.6) as a linear system for \mathfrak{U}_{n+1} , say $\mathfrak{D}\mathfrak{U}_{n+1} = \mathfrak{p}$ and $\mathfrak{N}\mathfrak{U}_{n+1} = \mathfrak{q}$ where \mathfrak{D} and \mathfrak{N} are the "matrix versions" of Dirichlet and Neumann operators, respectively, and \mathfrak{p} and \mathfrak{q} are the vector versions of the right-hand sides of the Dirichlet and Neumann conditions in (4.6), respectively. Regarding the regularization term, we define a matrix \mathfrak{S} such that $\mathfrak{S}\mathfrak{U}_{n+1}$ corresponds to $U_{n+1} + \sum_{|\alpha| \leq s} D^{\alpha} U_{n+1}$ where α is the usual multi-index. We refer the reader to [50,61,68] for details on the implementation of those matrices and vectors. We then need to minimize

$$\sum_{\mathbf{x}_{ij}\in\mathfrak{G}} \left[\left[\begin{array}{c} e^{2\lambda r^{-\beta}} \mathfrak{L} \\ \mathfrak{D} \\ \mathfrak{M} \end{array} \right] \mathfrak{U}_{n+1} - \left[\begin{array}{c} e^{2\lambda r^{-\beta}} \mathfrak{F} \\ \mathfrak{p} \\ \mathfrak{q} \end{array} \right] \right]^2 + \epsilon |\mathfrak{SU}_{n+1}|^2$$

for \mathfrak{U}_{n+1} . Hence, \mathfrak{U}_{n+1} solves the system

$$\left(\left[\begin{array}{ccc} e^{2\lambda r^{-\beta}}\mathfrak{Q}^{\mathrm{T}} & \mathfrak{D}^{\mathrm{T}} & \mathfrak{N}^{\mathrm{T}}\end{array}\right] \left[\begin{array}{ccc} e^{2\lambda r^{-\beta}}\mathfrak{Q} \\ \mathfrak{D} \\ \mathfrak{N} \end{array}\right] + \epsilon\mathfrak{S}^{\mathrm{T}}\mathfrak{S} \right) \mathfrak{U}_{n+1} = \left[\begin{array}{ccc} e^{2\lambda r^{-\beta}}\mathfrak{Q}^{\mathrm{T}} & \mathfrak{D}^{\mathrm{T}} & \mathfrak{N}^{\mathrm{T}}\end{array}\right] \left[\begin{array}{ccc} e^{2\lambda r^{-\beta}}\mathfrak{F} \\ \mathfrak{p} \\ \mathfrak{q} \end{array}\right].$$

In our Matlab script, we simply define

$$\mathfrak{U}_{n+1} = \operatorname{lsqlin} \left(\left[\begin{array}{ccc} e^{2\lambda r^{-\beta}} \mathfrak{V}^{\mathrm{T}} & \mathfrak{D}^{\mathrm{T}} & \mathfrak{N}^{\mathrm{T}} \end{array} \right] \left[\begin{array}{ccc} e^{2\lambda r^{-\beta}} \mathfrak{V} \\ \mathfrak{D} \\ \mathfrak{N} \end{array} \right] + \epsilon \mathfrak{S}^{\mathrm{T}} \mathfrak{S}, \left[\begin{array}{ccc} e^{2\lambda r^{-\beta}} \mathfrak{V}^{\mathrm{T}} & \mathfrak{D}^{\mathrm{T}} & \mathfrak{N}^{\mathrm{T}} \end{array} \right] \left[\begin{array}{ccc} e^{2\lambda r^{-\beta}} \mathfrak{F} \\ \mathfrak{p} \\ \mathfrak{q} \end{array} \right] \right)$$

where lsqlin is a build-in command of Matlab, used to solve linear systems. Again, the details of the implementation above to compute the regularized solution U_{n+1} to (4.6) respectively can be found in [50,61,68]. One can solve (4.5) using the same technique.

4.3. Numerical examples

Test 1. We test the case when the "donut-shaped" function f^{true} is given by

$$f^{\text{true}}(x, y) = \begin{cases} 2 & \text{if } 0.15^2 < (x - 0.35)^2 + y^2 < 0.6^2 \\ 1 & \text{otherwise} \end{cases} \text{ for all } (x, y) \in \Omega.$$

The true and computed source functions f are displayed in Fig. 1.

Fig. 1 illustrates that Algorithm 1 provides a satisfactory solution to Problem 1.1. By comparing the "donut"-shaped inclusions in both Fig. 1a and Fig. 1b, we conclude that the computation of the donut's shape and position is quite accurate. Furthermore, the maximum value of the function f within the computed donut is 1.765, which corresponds to a relative error of 11.73%. The approaching zero behavior of the curve in Fig. 1c numerically demonstrates the convergence of the Carleman contraction method.

Test 2. We consider an intriguing case f^{true} whose graphs feature an " Σ " shape. The true value of the function $f^{\text{true}}(x,y)=2$ if the point (x,y) in the letter Σ . Otherwise, $f^{\text{true}}(x,y)=1$. The true and computed source functions f are displayed in Fig. 2.

Fig. 2 presents a numerical solution that is satisfactory for Problem 1.1. The letter " Σ " and its position are accurately reconstructed. The maximum value of the function f inside the computed " Σ " is 1.8454, representing a relative error of 7.73%. Similar to Test 1, the convergence of the Carleman contraction method is numerically confirmed by Fig. 2c.

Test 3. We test a similar experiment to the source function f in Test 2. The function f^{true} has a graph looking like the letter " Ω ." The true value of the function $f^{\text{true}}(x,y)=2$ if the point (x,y) in the letter Ω . Otherwise, $f^{\text{true}}(x,y)=1$. The true and computed source functions f are displayed in Fig. 3.

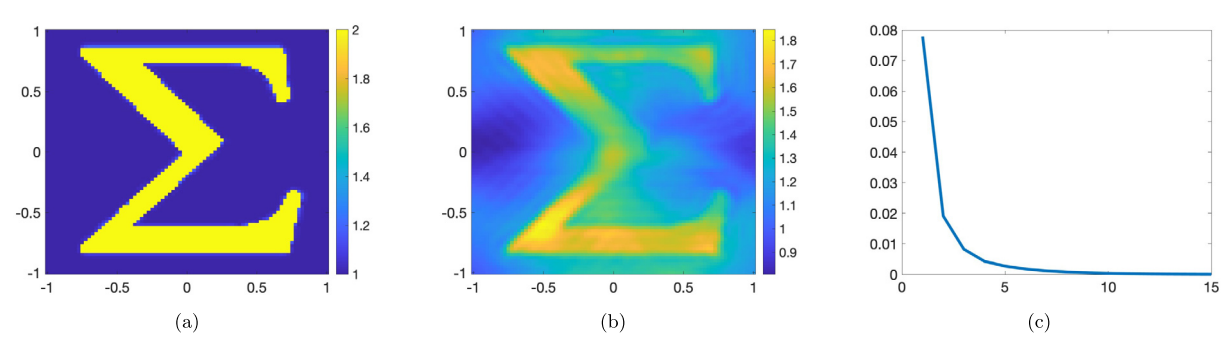


Fig. 2. (a) and (b) the true and computed initial condition f^{true} and f^{comp} respectively; (c) the consecutive relative difference $\frac{\|U_{n+1}-U_n\|_{L^{\infty}(\Omega)}}{\|U_n\|_{L^{\infty}(\Omega)}}$. The horizontal axis of this figure is the number of iteration n. The boundary data used to reconstruct the function f is corrupted with $\delta = 0.1$.

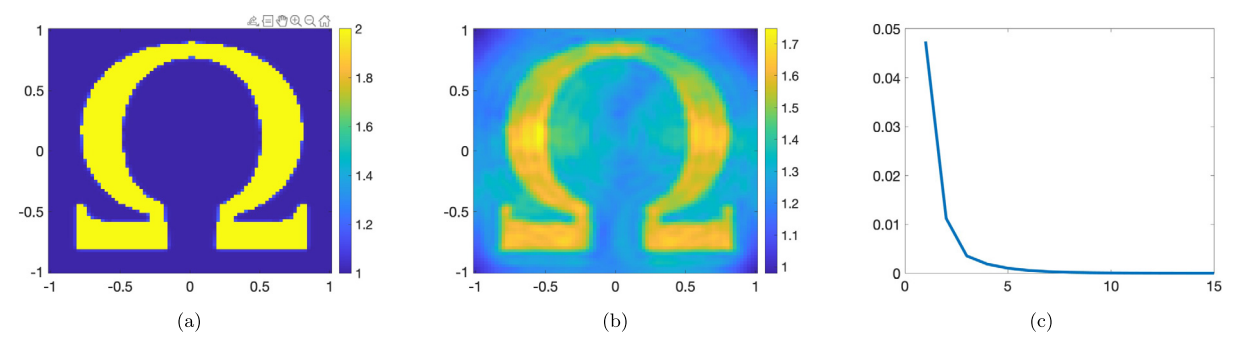


Fig. 3. (a) and (b) the true and computed initial condition f^{true} and f^{comp} respectively; (c) the consecutive relative difference $\frac{\|U_{n+1}-U_n\|_{L^{\infty}(\Omega)}}{\|U_n\|_{L^{\infty}(\Omega)}}$. The horizontal axis of this figure is the number of iteration n. The boundary data used to reconstruct the function f is corrupted with $\delta = 0.1$.

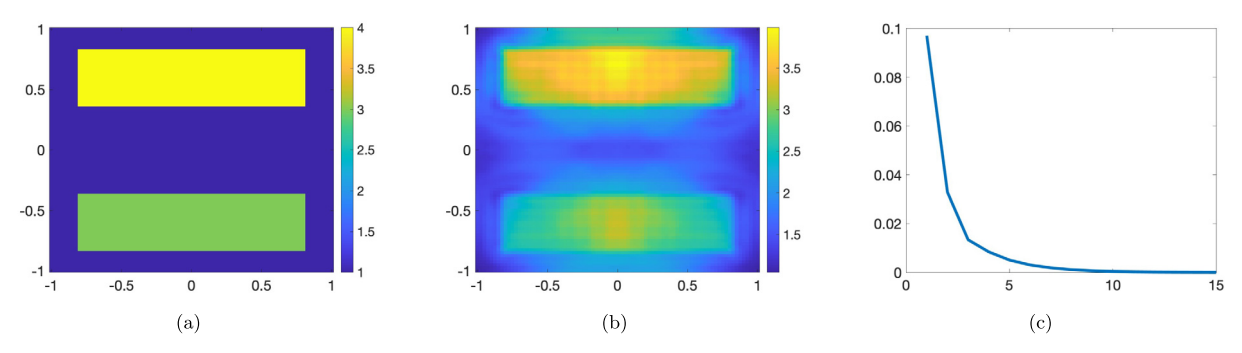


Fig. 4. (a) and (b) the true and computed initial condition f^{true} and f^{comp} respectively; (c) the consecutive relative difference $\frac{\|U_{n+1}-U_n\|_{L^{\infty}(\Omega)}}{\|U_n\|_{L^{\infty}(\Omega)}}$. The horizontal axis of this figure is the number of iteration n. The boundary data used to reconstruct the function f is corrupted with $\delta = 0.1$.

Fig. 3 presents a numerical solution that is satisfactory for Problem 1.1. The letter " Ω " and its position are accurately reconstructed. The maximum value of the function f inside the computed " Ω " is 1.7473, representing a relative error of 12.64%. The convergence of the Carleman contraction method is numerically confirmed by Fig. 3c.

Test 4. In this test, we consider a more complicated circumstance in which the graph of the true function f has two "inclusions". Each inclusion looks like a horizontal line segment. The value of function f^{true} is 4 in the line on the top and 3 inside the line in the bottom. The true and computed source functions f are displayed in Fig. 4.

Our algorithm works well for this test. It is evident that both "horizontal inclusions" are successfully identified. The peak value of the computed function f inside the "top" inclusion is 3.9845 (relative error 0.39%). The peak value of the computed function f inside the "bottom" inclusion is 3.25782 (relative error 8.59%).

Remark 4.1. To emphasize that our method is independent of the unknown damping coefficient a, we use different a in the tests above.

1. The unknown function a^{true} in Test 1 is given by

$$a^{\mathrm{true}}(x,y) = \left\{ \begin{array}{ll} 2e^{\frac{x^2+y^2}{x^2+y^2-1}} & \text{if } x^2+y^2 < 1 \\ 0 & \text{otherwise,} \end{array} \right. \quad \text{for all } (x,y) \in \Omega.$$

2. The unknown function a^{true} in Test 2 is given by

$$a^{\text{true}}(x, y) = |y^2 - x|$$
 for all $(x, y) \in \Omega$.

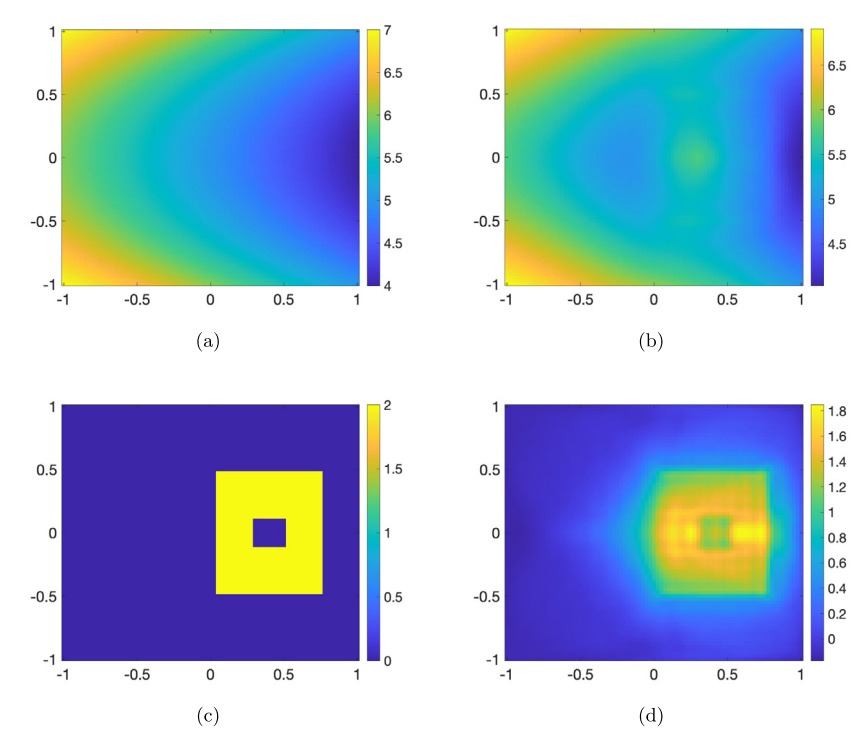


Fig. 5. (a) and (b) the true and computed initial conditions f respectively; (c) and (d) the true and computed damping coefficients a respectively. The data incorporated in this test includes a noise level of 10%.

3. The unknown function a^{true} in Test 3 is given by

$$a^{\text{true}}(x, y) = x^2$$
 for all $(x, y) \in \Omega$.

4. The unknown function a^{true} in Test 4 is given by

$$a^{\text{true}}(x, y) = \begin{cases} 2e^{\frac{r^2}{r^2 - 1}} & \text{if } r < 1\\ 0 & \text{otherwise,} \end{cases} \text{ for all } (x, y) \in \Omega,$$
 where $r = r(x, y) = \sqrt{\frac{x^2}{0.5^2} + \frac{y^2}{0.25^2}}$.

Remark 4.2. Figs. 1c through 4c present the graphs of the function $n \mapsto \frac{\|U_{n+1} - U_n\|_{L^{\infty}(\Omega)}}{\|U_n\|_{L^{\infty}(\Omega)}}$, representing the relative difference between consecutive estimations of U_n as calculated within the loop from Step 4 to Step 10 in Algorithm 1. These figures provide numerical evidence for the convergence of Algorithm 1 as n approaches infinity. It is important to note that this convergence leads to an approximation of the actual solution U^* to the equation (3.10), not the function $f(\mathbf{x})$.

Upon calculating the vector value $U^{\text{comp}} = (u_1^{\text{comp}}, \dots, u_N^{\text{comp}})$ at Step 11, one might intuitively consider the problem of reconstructing the unknown coefficient a(x,y), $(x,y) \in \Omega$, by combining equations (2.1) and (2.3). More precisely, one could suggest the following formula

$$a(x,y) = -\frac{\left[\sum_{l=1}^{N} u_{l}^{\text{comp}}(x,y)\Psi_{l}'(0)\right] \left[\sum_{l=1}^{N} u_{l}^{\text{comp}}(x,y)\Psi_{l}(0)\right]}{\left|\sum_{l=1}^{N} u_{l}^{\text{comp}}(x,y)\Psi_{l}(0)\right|^{2} + \eta^{2}} \quad \text{for all } (x,y) \in \Omega.$$

$$(4.7)$$

However, we find that equation (4.7) is not universally successful. Our numerical observations suggest that its applicability is heavily contingent on the nature of the function f^{true} . If f^{true} is smooth, equation (4.7) can reliably reconstruct the coefficient a. Conversely, if f^{true} lacks continuity, the formula presented in (4.7) fails. In the next two tests, we show the reconstruction of both f and a when f is smooth.

Test 5. In this test, we set

$$f^{\text{true}}(x, y) = y^2 - x + 5$$

and

$$a^{\text{true}}(x,y) = \begin{cases} 0 & \text{if } \max\{\sqrt{2}|x-0.4|,|y|\} > 0.5 \text{ or } \max\{|x-0.4|,|y|\}_1 < 0.12, \\ 2 & \text{otherwise,} \end{cases}$$

for all $(x, y) \in \Omega$. The true and reconstructed of these functions are displayed in Fig. 5.

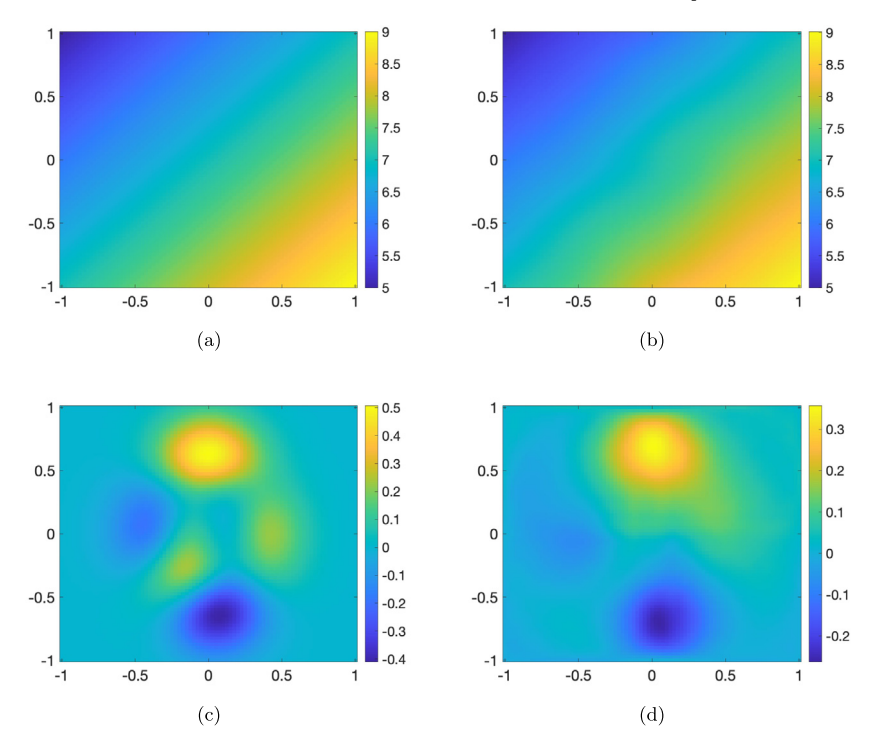


Fig. 6. (a) and (b) the true and computed initial conditions f respectively; (c) and (d) the true and computed damping coefficients a respectively. The data incorporated in this test includes a noise level of 10%.

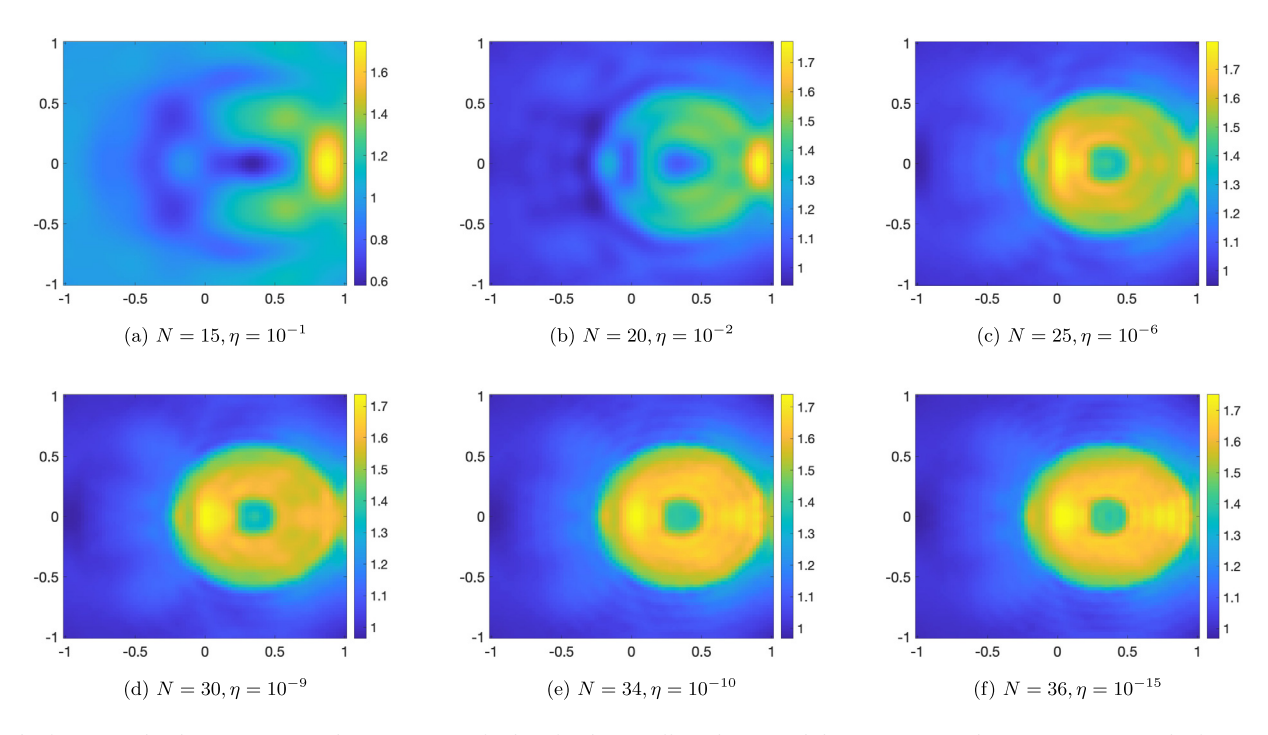


Fig. 7. The function f has been reconstructed using a range of values for the cut-off number N and the parameter η . The reconstructions in the first row do not meet expectations due to inappropriate selections of these two parameters. However, the reconstructions' accuracy in the second row, achieved with a large N and a small η , alongside the reconstruction of f shown in Fig. 1b (where N=35 and $\eta=10^{-11}$), numerically demonstrates our method's convergence when these parameters are properly chosen. The data in this experiment is generated in Test 1.

The relative error for the initial condition, calculated as $\frac{\|f^{\text{comp}}-f^{\text{true}}\|_{L^2(\Omega)}}{\|f^{\text{true}}\|_{L^2(\Omega)}}$, is 5.47%, which falls below the noise level. Although the L^2 relative error in calculating the damping coefficient a is large, the reconstructed maximum value of a within the inclusion resembling a square with a void is still considered acceptable. Inside the inclusion, the computed maximum value of a^{comp} is 1.8474, corresponding to a relative error of 7.63%. **Test 6.** In this test, we set

and

$$a^{\text{true}}(x,y) = \frac{1}{16} \left[3(1-3x)^2 e^{-3x^2 - (2.5y+1)^2} - 10\left(\frac{3x}{5} - 27x^3 - 97.6562y^5\right) e^{-9x^2 - 6.25y^2} - \frac{e^{-(3x+1)^2 - 6.25y^2}}{3} \right]$$

for all $(x, y) \in \Omega$. This test is interesting since we are solving a nonlinear problem when the values of the unknown f are high and the formula of the unknown g is very complicated. Both unknowns function are continuous. The true and reconstructed of these functions are displayed in Fig. 6.

The relative error for the initial condition, calculated as $\frac{\|\int^{\text{comp}}-\int^{\text{true}}\|L^2(\Omega)}{\|\int^{\text{true}}\|L^2(\Omega)}$, is 0.62%, which is very impressive. As in Test 5, the L^2 relative error in calculating the damping coefficient a is large. However, the visual reconstruction of a meets the expectation. One can see all peaks in the graph of the function a^{comp} .

Remark 4.3. Our Algorithm 1 relies on two key elements: using an approximation model (2.12) with a regularization parameter η , as shown in (2.3), and applying a cutoff number N for truncation in (2.3). However, as mentioned in Remark 2.3, this model and method are approximations, not exact. Therefore, it is important to test how well our method works when we use large values of N and small values of η . To do this, we run tests with various N and η values to observe the convergence. The results, shown in Fig. 7, confirm our desired convergence.

Data availability

Data will be made available on request.

Acknowledgement

The works of TTL and LHN were partially supported by National Science Foundation grant DMS-2208159, by funds provided by the Faculty Research Grant program at UNC Charlotte Fund No. 111272, and by the CLAS small grant provided by the College of Liberal Arts & Sciences, UNC Charlotte. The works of HP were supported in part by National Science Foundation grant DMS-2150179. LVN was partially supported by the National Science Foundation grant DMS-1616904. We thank the anonymous referees for their constructive comments which helped to improve the presentation of the paper

References

- [1] S. Acosta, B. Palacios, Thermoacoustic tomography for an integro-differential wave equation modeling attenuation, J. Differ. Equ. 5 (2018) 1984-2010.
- [2] H. Ammari, E. Bretin, J. Garnier, V. Wahab, Time reversal in attenuating acoustic media, Contemp. Math. 548 (2011) 151-163.
- [3] H. Ammari, E. Bretin, E. Jugnon, V. Wahab, Photoacoustic imaging for attenuating acoustic media, in: H. Ammari (Ed.), Mathematical Modeling in Biomedical Imaging II, Springer, 2012 pp. 57–84
- [4] A.B. Bakushinskii, M.V. Klibanov, N.A. Koshev, Carleman weight functions for a globally convergent numerical method for ill-posed Cauchy problems for some quasilinear PDEs, Nonlinear Anal., Real World Appl. 34 (2017) 201–224.
- [5] L. Beilina, M.V. Klibanov, Approximate Global Convergence and Adaptivity for Coefficient Inverse Problems, Springer, New York, 2012.
- [6] Zakaria Belhachmi, Thomas Glatz, Otmar Scherzer, A direct method for photoacoustic tomography with inhomogeneous sound speed, Inverse Probl. 32 (4) (2016) 045005.
- [7] A.L. Bukhgeim, M.V. Klibanov, Uniqueness in the large of a class of multidimensional inverse problems, Sov. Math. Dokl. 17 (1981) 244-247.
- [8] P. Burgholzer, H. Grün, M. Haltmeier, R. Nuster, G. Paltauf, Compensation of acoustic attenuation for high-resolution photoa- coustic imaging with line detectors, Proc. SPIE 6437 (2007) 643724.
- [9] C. Clason, M.V. Klibanov, The quasi-reversibility method for thermoacoustic tomography in a heterogeneous medium, SIAM J. Sci. Comput. 30 (2007) 1–23.
- [10] N. Do, L. Kunyansky, Theoretically exact photoacoustic reconstruction from spatially and temporally reduced data, Inverse Probl. 34 (9) (2018) 094004.
- [11] David Finch, Sarah K. Patch, Determining a function from its mean values over a family of spheres, SIAM J. Math. Anal. 35 (5) (2004) 1213–1240.
- [12] David Finch, Markus Haltmeier, Rakesh, Inversion of spherical means and the wave equation in even dimensions, SIAM J. Appl. Math. 68 (2) (2007) 392-412.
- [13] M. Haltmeier, Inversion of circular means and the wave equation on convex planar domains, Comput. Math. Appl. 65 (2013) 1025–1036.
- [14] Markus Haltmeier, Linh V. Nguyen, Analysis of iterative methods in photoacoustic tomography with variable sound speed, SIAM J. Imaging Sci. 10 (2) (2017) 751–781.
- [15] M. Haltmeier, L.V. Nguyen, Reconstruction algorithms for photoacoustic tomography in heterogeneous damping media, J. Math. Imaging Vis. 61 (2019) 1007–1021. [16] Markus Haltmeier, Richard Kowar, Linh V. Nguyen, Iterative methods for photoacoustic tomography in attenuating acoustic media, Inverse Probl. 33 (11) (2017) 115009.
- [17] M. Hanke, A. Neubauer, O. Scherzer, A convergence analysis of the Landweber iteration for nonlinear ill-posed problems, Numer. Math. 72 (1995) 21–37.
- [18] D.N. Hào, T.T. Le, L.H. Nguyen, The dimensional reduction method for solving a nonlinear inverse heat conduction problem with limited boundary data, Commun. Nonlinear Sci. Numer. Simul. 128 (2024) 107679.
- [19] A. Homan, Multi-wave imaging in attenuating media, Inverse Probl. Imaging 7 (2013) 1235–1250.
- [20] Y. Hristova, Time reversal in thermoacoustic tomography-an error estimate, Inverse Probl. 25 (2009) 055008.
- [21] Y. Hristova, P. Kuchment, L.V. Nguyen, Reconstruction and time reversal in thermoacoustic tomography in acoustically homogeneous and inhomogeneous media, Inverse Probl. 24 (2008) 055006.
- [22] C. Huang, K. Wang, L. Nie, L.V. Wang, M.A. Anastasio, Full-wave iterative image reconstruction in photoacoustic tomography with acoustically inhomogeneous media, IEEE Trans. Med. Imaging 32 (2013) 1097–1110.
- [23] V. Katsnelson, L.V. Nguyen, On the convergence of time reversal method for thermoacoustic tomography in elastic media, Appl. Math. Lett. 77 (2018) 79-86.
- [24] Peter Kuchment, The Radon Transform and Medical Imaging, Society for Industrial and Applied Mathematics, 2013.
- [25] Peter Kuchment, Leonid Kunyansky, Mathematics of thermoacoustic tomography, Eur. J. Appl. Math. 19 (2) (2008) 191–224.
- [26] Leonid A. Kunyansky, Explicit inversion formulae for the spherical mean Radon transform, Inverse Probl. 23 (1) (2007) 373.
- [27] V.A. Khoa, G.W. Bidney, M.V. Klibanov, L.H. Nguyen, L. Nguyen, A. Sullivan, V.N. Astratov, Convexification and experimental data for a 3D inverse scattering problem with the moving point source, Inverse Probl. 36 (2020) 085007.
- [28] V.A. Khoa, G.W. Bidney, M.V. Klibanov, L.H. Nguyen, L. Nguyen, A. Sullivan, V.N. Astratov, An inverse problem of a simultaneous reconstruction of the dielectric constant and conductivity from experimental backscattering data, Inverse Probl. Sci. Eng. 29 (5) (2021) 712–735.
- [29] V.A. Khoa, M.V. Klibanov, L.H. Nguyen, Convexification for a 3D inverse scattering problem with the moving point source, SIAM J. Imaging Sci. 13 (2) (2020) 871-904.
- [30] M.V. Klibanov, Global convexity in a three-dimensional inverse acoustic problem, SIAM J. Math. Anal. 28 (1997) 1371–1388.
- [31] M.V. Klibanov, Global convexity in diffusion tomography, Nonlinear World 4 (1997) 247–265.
- [32] M.V. Klibanov, Carleman weight functions for solving ill-posed Cauchy problems for quasilinear PDEs, Inverse Probl. 31 (2015) 125007.
- [33] M.V. Klibanov, Convexification of restricted Dirichlet to Neumann map, J. Inverse Ill-Posed Probl. 25 (5) (2017) 669–685.
- [34] M.V. Klibanov, O.V. Ioussoupova, Uniform strict convexity of a cost functional for three-dimensional inverse scattering problem, SIAM J. Math. Anal. 26 (1995) 147–179.
- [35] M.V. Klibanov, A.E. Kolesov, Convexification of a 3-D coefficient inverse scattering problem, Comput. Math. Appl. 77 (2019) 1681–1702.
- [36] M.V. Klibanov, T.T. Le, L.H. Nguyen, A. Sullivan, L. Nguyen, Convexification-based globally convergent numerical method for a 1D coefficient inverse problem with experimental data, Inverse Probl. Imaging 16 (2022) 1579–1618.

- [37] M.V. Klibanov, J. Li, Inverse Problems and Carleman Estimates: Global Uniqueness, Global Convergence and Experimental Data, De Gruyter, 2021.
- [38] M.V. Klibanov, J. Li, W. Zhang, Convexification of electrical impedance tomography with restricted Dirichlet-to-Neumann map data, Inverse Probl. 35 (2019) 035005.
- [39] M.V. Klibanov, Z. Li, W. Zhang, Convexification for the inversion of a time dependent wave front in a heterogeneous medium, SIAM J. Appl. Math. 79 (2019) 1722–1747.
- [40] M.V. Klibanov, L.H. Nguyen, PDE-based numerical method for a limited angle X-ray tomography, Inverse Probl. 35 (2019) 045009.
- [41] M.V. Klibanov, L.H. Nguyen, H.V. Tran, Numerical viscosity solutions to Hamilton-Jacobi equations via a Carleman estimate and the convexification method, J. Comput. Phys. 451 (2022) 110828.
- [42] R. Kowar, On time reversal in photoacoustic tomography for tissue similar to water, SIAM J. Imaging Sci. 7 (2014) 509-527.
- [43] R. Kowar, O. Scherzer, Photoacoustic imaging taking into account attenuation, in: H. Ammari (Ed.), Mathematics and Algorithms in Tomography II, in: Lecture Notes in Mathematics, Springer, 2012, pp. 85–130.
- [44] R.A. Kruger, P. Liu, Y.R. Fang, C.R. Appledorn, Photoacoustic ultrasound (PAUS)-reconstruction tomography, Med. Phys. 22 (1995) 1605.
- [45] R.A. Kruger, D.R. Reinecke, G.A. Kruger, Thermoacoustic computed tomography: technical considerations, Med. Phys. 26 (1999) 1832.
- [46] R. Lattès, J.L. Lions, The Method of Quasireversibility: Applications to Partial Differential Equations, Elsevier, New York, 1969.
- [47] M.M. Lavrent'ev, V.G. Romanov, S.P. Shishatskii, Ill-Posed Problems of Mathematical Physics and Analysis, Translations of Mathematical Monographs, AMS, Providence, RI, 1986.
- [48] T.T. Le, Global Reconstruction of Initial Conditions of Nonlinear Parabolic Equations via the Carleman-Contraction Method, Advances in Inverse Problems for Partial Differential Equations, vol. 784, Amer. Math. Soc., 2023, pp. 145–167.
- [49] T.T. Le, V.A. Khoa, M.V. Klibanov, L.H. Nguyen, G.W. Bidney, V.N. Astratov, Numerical verification of the convexification method for a frequency-dependent inverse scattering problem with experimental data, J. Appl. Ind. Math. (2023), preprint, arXiv:2306.00761, in press.
- [50] T.T. Le, L.H. Nguyen, A convergent numerical method to recover the initial condition of nonlinear parabolic equations from lateral Cauchy data, J. Inverse Ill-Posed Probl. 30 (2) (2022) 265–286.
- [51] T.T. Le, L.H. Nguyen, The gradient descent method for the convexification to solve boundary value problems of quasi-linear PDEs and a coefficient inverse problem, J. Sci. Comput. 91 (3) (2022) 74.
- [52] T.T. Le, L.H. Nguyen, T-P. Nguyen, W. Powell, The quasi-reversibility method to numerically solve an inverse source problem for hyperbolic equations, J. Sci. Comput. 87 (2021) 90.
- [53] T.T. Le, L.H. Nguyen, H.V. Tran, A Carleman-based numerical method for quasilinear elliptic equations with over-determined boundary data and applications, Comput. Math. Appl. 125 (2022) 13–24.
- [54] Hongyu Liu, Gunther Uhlmann, Determining both sound speed and internal source in thermo- and photo-acoustic tomography, Inverse Probl. 31 (10) (2015) 105005.
- [55] Thomas P. Matthews, et al., Parameterized joint reconstruction of the initial pressure and sound speed distributions for photoacoustic computed tomography, SIAM J. Imaging Sci. 11 (2) (2018) 1560–1588.
- [56] A.I. Nachman, J.F. Smith III, R.C. Waag, An equation for acoustic propagation in inhomogeneous media with relaxation losses, J. Acoust. Soc. Am. 88 (1990) 1584–1595.
- [57] F. Natterer, Photo-acoustic inversion in convex domains, Inverse Probl. Imaging 6 (2012) 315-320.
- [58] D-L. Nguyen, L.H. Nguyen, T. Truong, The Carleman-based contraction principle to reconstruct the potential of nonlinear hyperbolic equations, Comput. Math. Appl. 128 (2022) 239–248.
- [59] H.M. Nguyen, L.H. Nguyen, Cloaking using complementary media for the Helmholtz equation and a three spheres inequality for second order elliptic equations, Trans. Am. Math. Soc. 2 (2015) 93–112.
- [60] L.H. Nguyen, An inverse space-dependent source problem for hyperbolic equations and the Lipschitz-like convergence of the quasi-reversibility method, Inverse Probl. 35 (2019) 035007
- [61] L.H. Nguyen, A new algorithm to determine the creation or depletion term of parabolic equations from boundary measurements, Comput. Math. Appl. 80 (2020) 2135-2149.
- [62] L.H. Nguyen, The Carleman contraction mapping method for quasilinear elliptic equations with over-determined boundary data, Acta Mathematica Vietnamica, DOI, https://doi.org/10.1007/s40306-023-00500-w, 2023.
- [63] L.H. Nguyen, M.V. Klibanov, Carleman estimates and the contraction principle for an inverse source problem for nonlinear hyperbolic equations, Inverse Probl. 38 (2022) 035009.
- [64] L.H. Nguyen, Q. Li, M.V. Klibanov, A convergent numerical method for a multi-frequency inverse source problem in inhomogenous media, Inverse Probl. Imaging 13 (2019) 1067–1094.
- [65] L.H. Nguyen, H.T. Vu, Reconstructing a space-dependent source term via the quasi-reversibility method, in: D-L. Nguyen, L.H. Nguyen, T-P. Nguyen (Eds.), Advances in Inverse Problems for Partial Differential Equations, in: Contemporary Mathematics, vol. 748, American Mathematical Society, 2023, pp. 103–118.
- [66] L.V. Nguyen, A family of inversion formulas in thermoacoustic tomography, Inverse Probl. Imaging 3 (2009) 649–675.
- [67] P.M. Nguyen, T.T. Le, L.H. Nguyen, M.V. Klibanov, Numerical differentiation by the polynomial-exponential basis, Journal of Applied and Industrial Mathematics, in press, preprint, arXiv:2304.05909, 2023.
- [68] P.M. Nguyen, L.H. Nguyen, A numerical method for an inverse source problem for parabolic equations and its application to a coefficient inverse problem, J. Inverse Ill-Posed Probl. 38 (2020) 232–339.
- [69] A. Oraevsky, S. Jacques, R. Esenaliev, F. Tittel, Laser-based optoacoustic imaging in biological tissues, Proc. SPIE 2134A (1994) 122.
- [70] Benjamin Palacios, Reconstruction for multi-wave imaging in attenuating media with large damping coefficient, Inverse Probl. 32 (12) (2016) 125008.
- [71] Benjamin Palacios, Photoacoustic tomography in attenuating media with partial data, Inverse Probl. Imaging 16 (5) (2022) 1085-1111.
- [72] G. Paltauf, R. Nuster, M. Haltmeier, P. Burgholzer, Experimental evaluation of reconstruction algorithms for limited view photoacoustic tomography with line detectors, Inverse Probl. 23 (2007) S81–S94.
- [73] G. Paltauf, J.A. Viator, S.A. Prahl, S.L. Jacques, Iterative reconstruction algorithm for optoacoustic imaging, J. Opt. Soc. Am. 112 (2002) 1536-1544.
- [74] A.V. Smirnov, M.V. Klibanov, L.H. Nguyen, On an inverse source problem for the full radiative transfer equation with incomplete data, SIAM J. Sci. Comput. 41 (2019) B929-B952.
- [75] P. Stefanov, G. Uhlmann, Thermoacoustic tomography with variable sound speed, Inverse Probl. 25 (2009) 075011.
- [76] P. Stefanov, G. Uhlmann, Thermoacoustic tomography arising in brain imaging, Inverse Probl. 27 (2011) 045004.
- [77] Plamen Stefanov, Gunther Uhlmann, Recovery of a source term or a speed with one measurement and applications, Trans. Am. Math. Soc. 365 (11) (2013) 5737–5758.
- [78] Plamen D. Stefanov, Gunther Uhlmann, Instability of the linearized problem in multiwave tomography of recovery both the source and the speed, Inverse Probl. Imaging 7 (4) (2013) 1367.
- [79] Minghua Xu, Lihong V. Wang, Photoacoustic imaging in biomedicine, Rev. Sci. Instrum. 77 (2006) 4.
- [80] Jin Zhang, Mark A. Anastasio, Reconstruction of Speed-of-Sound and Electromagnetic Absorption Distributions in Photoacoustic Tomography, Photons Plus Ultrasound: Imaging and Sensing 2006: The Seventh Conference on Biomedical Thermoacoustics, Optoacoustics, and Acousto-Optics, vol. 6086, SPIE, 2006.